RSC Medicinal Chemistry



RESEARCH ARTICLE

View Article Online
View Journal | View Issue



Cite this: RSC Med. Chem., 2024, 15, 595

Formulation of a fast-disintegrating drug delivery system from cyclodextrin/naproxen inclusion complex nanofibrous films†

Asli Celebioglu, ¹ Bareena Dash, ¹ Mahmoud Aboelkheir, ¹ Mehmet E. Kilic, ¹ Engin Durgun ¹ and Tamer Uyar ¹ And Tamer ¹ And

Naproxen is a well-known non-steroidal anti-inflammatory drug (NSAID) that suffers from limited water solubility. The inclusion complexation with cyclodextrin (CD) can eliminate this drawback and the free-standing nanofibrous film (NF) generated from these inclusion complexes (ICs) can be a promising alternative formula as an orally disintegrating drug delivery system. For this, naproxen/CD IC NFs were generated using the highly water soluble hydroxypropylated derivative of β CD (HP β CD) with two different molar ratios of 1/1 and 1/2 (drug/CD). The complexation energy calculated by the modeling study demonstrated a more favorable interaction between HP β CD and naproxen for the 1/2 molar ratio than 1/1. HP β CD/naproxen IC NFs were generated with loading concentrations of \sim 7–11% and without using toxic chemicals. HP β CD/naproxen IC NFs indicated a faster and enhanced release profile in aqueous medium compared to pure naproxen owing to inclusion complexation. Moreover, rapid disintegration in less than a second was achieved in an artificial saliva environment.

Received 5th October 2023, Accepted 17th December 2023

DOI: 10.1039/d3md00557g

rsc.li/medchem

Introduction

One of the major issues in the pharmaceutical industry is the rising number of poorly water-soluble drugs and their low bioavailability to the human body. Over 70% of new chemical entities in the drug discovery pipeline are nearly insoluble in water, leading to slow drug absorption, gastrointestinal toxicity, and insufficient bioavailability. ^{1,2} In response to this problem, fast-disintegrating oral drug delivery systems have gained an increasing amount of attention due to their ability to provide rapid and enhanced drug absorption and improved bioavailability by reducing the hepatic first-pass effect. ^{3,4} Fast-disintegrating systems can be in flexible, thin, and free-standing strip/film forms having hygroscopic profiles which enable the dissolution of these systems in a moist environment by eliminating the use of water. Here, the fast disintegration of the delivery system in the oral mucosa

For developing water-soluble nanofibrous films with quick disintegration times, different types of natural and synthetic hydrophilic polymers have been employed including polyvinyl alcohol (PVA),^{14,15} poly(ethylene oxide) (PEO),¹⁵ polyvinylpyrrolidone (PVP),^{15,16} pullulan,^{17,18} *etc.* just as used for commercially available orally disintegrating films (ODFs).¹⁹ However, toxic solvents, additional chemicals or high processing temperature might be required for proper incorporation of drug molecules into electrospun polymer

removes the choking hazard and need for swallowing which results in a rise in patient compliance.3-5 Therefore, fastdisintegrating oral drug delivery systems are useful alternative pharmaceutical forms to tablets and capsules. Fastdisintegrating systems can be generated through processes such as freeze drying, granulation, molding, compression, spraying, etc. which are meant to enhance the dissolution rate and thus, the bioavailability of the drugs. On the other hand, the technique of electrospinning has become a prominent approach for engineering nanomaterials in the form of freestanding fibrous films as carriers of chemical and biological compounds in therapeutic applications.⁷⁻⁹ The unique properties of electrospun nanofibers such as highly porous structure, high surface area, being lightweight and drug encapsulation capability make these fibrous films attractive for the emerging orally fast-disintegrating delivery system.¹⁰ Moreover, the potential of these nanofibrous films can be verified by using different configurations of electrospinning such as coaxial,11 triaxial12 and side-by-side.13

 ^a Fiber Science Program, Department of Human Centered Design, College of Human Ecology, Cornell University, Ithaca, NY, 14853, USA. E-mail: tu46@cornell.edu
 ^b Biological Sciences, College of Arts and Sciences, Cornell University, Ithaca, NY, 14853, USA

^c Computational Science Research Center, Korea Institute of Science and Technology, Seoul, 02792, Republic of Korea

^d UNAM-National Nanotechnology Research Center and Institute of Materials Science and Nanotechnology, Bilkent University, Ankara 06800, Turkey

 $[\]dagger$ Electronic supplementary information (ESI) available. See DOI: https://doi.org/10.1039/d3md00557g

matrices. At this point, cyclodextrin (CD) drug inclusion complexes electrospun into nanofibrous films without using a polymer or another toxic chemical can circumvent the problems present in polymer-based drug carrier systems.²⁰⁻²⁷ CDs, playing a key role in drug encapsulation, are a class of oligosaccharides derived from starch. CDs are non-toxic and bio-safe molecules having a donut shape which enables the formation of inclusion complexes with various hydrophobic compounds by encapsulating them into the relatively hydrophobic inner cavity of CDs. Here, the inclusion complexation can increase the water solubility, bioavailability, and stability of the encapsulated bioactive compounds and this ensures a widespread application for CDs and their inclusion complexes particularly across the medicine, pharmacy, and biotechnology areas. 10,28,29

Research Article

Naproxen is a non-steroidal anti-inflammatory drug (NSAID) that is used to reduce the inflammation, fever and pain during the treatment of migraine, arthritis, kidney stones, gout, menstrual cramps, etc. However, the poorly water-soluble nature of naproxen limits its use for pharmaceutical administration.³⁰ As was reported previously, this shortcoming of naproxen can be dissolved by forming inclusion complexes with different types of CD molecules.30-37 Even, in a related study by Séon-Lutz et al., hyaluronic acid/PVA nanofibers were incorporated with the inclusion complexes of hydroxypropyl-beta-cyclodextrin (HPβCD) and naproxen for the purpose of wound dressing applications.³⁸ In another study reported by the Uyar group, poly(ε-caprolactone) (PCL) nanofibers were functionalized with naproxen/βCD inclusion complexes that provided an enhanced release profile for the drug molecule compared to the CD-free system.³⁹ In this study, HPBCD was used to form inclusion complexes with naproxen and then for the electrospinning of this complex system in the absence of any polymer or organic solvents (Fig. 1). The potential and the favourableness of naproxen/HPβCD inclusion complex nanofibrous films as a fast-disintegrating delivery system were revealed using morphological, structural, pharmacotechnical characterization techniques.

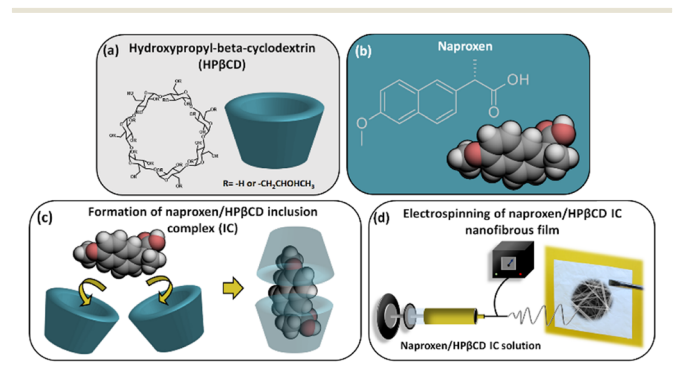


Fig. 1 Chemical structure of (a) hydroxypropyl-beta-cyclodextrin (HPβCD) and (b) naproxen. Schematic representation of (c) inclusion complex formation between naproxen and HPBCD molecules and (d) electrospinning of a naproxen/HPβCD IC nanofibrous film.

Experimental

Materials

Naproxen (99.3%, MP Biomedicals), buffer chemicals (phosphate buffered saline tablet (Sigma Aldrich), sodium phosphate dibasic heptahydrate (Na₂HPO₄, 98.0-102.0%, Fisher Chemical), sodium chloride (NaCl, >99%, Sigma-Aldrich), monobasic potassium phosphate (KH₂PO₄, ≥99.0%, Fisher Chemical), o-phosphoric acid (85%, Fisher Chemical), hydrochloric acid (Sigma-Aldrich, Ph. Eur., BP, NF, fuming, 36.5–38%), dimethyl sulfoxide (DMSO, certified ACS, Fisher Chemical) and deuterated dimethyl sulfoxide (DMSO-d₆, deuteration degree min. 99.8%, Cambridge Isotope) were obtained commercially. Hydroxypropyl-betacyclodextrin (HPβCD) (Cavasol® W7 HP, standard grade, molar substitution degree: ~0.9) was gifted from Wacker Chemie AG (USA). A Millipore Milli-Q ultrapure water system was used for distilled water.

Preparation of inclusion complex systems and electrospinning process

Clear solutions of HPBCD were prepared with a CD concentration of 180% (w/w, with respect to solvent) in distilled water (500 µL). Afterwards, naproxen was added to the clear HPβCD solutions to separately attain 1/1 and 1/2 molar ratios (drug/CD) that corresponded to ~13.3% (w/w, with respect to the total sample amount) and $\sim 7.1\%$ (w/w) naproxen content in ultimate nanofibrous films. To form inclusion complexes (ICs), the naproxen/HPβCD solutions were stirred overnight at RT. Pure HPβCD solution (180% (w/ w)) was prepared as the control sample. The conductivity and viscosity of all these aqueous systems were determined prior the electrospinning procedure. The conductivity of solutions was measured using a conductivity meter (FiveEasy, Mettler Toledo, USA), while viscosity was measured using a rheometer (AR 2000 rheometer, TA Instrument, USA, coneplate spindle (20 mm, 4°), shear rate (0.01–1000 s⁻¹)). The electrospinning solutions of naproxen/HPBCD ICs and pure HPβCD were individually transferred to a 1 mL plastic syringe fixed with 27 G needles. The electrospinning process was conducted in electrospinning equipment (Spingenix, model: SG100, Palo Alto, USA). For this, the solution loaded syringes were placed on a syringe pump and pushed with a flow rate of 0.3 mL h⁻¹. The high voltage power source was set to 17.5 kV to apply voltage to the needle for the deposition of nanofibers on the fixed metal collector. During the process, the relative humidity and temperature were recorded at around 26% and 20 °C, respectively.

Structural characterization

The morphology of naproxen/HPβCD (1/1) IC, naproxen/ HPβCD (1/2) IC and HPβCD nanofibrous films was examined through scanning electron microscopy (SEM, Tescan MIRA3, Czech Republic). Prior to the measurement, samples fixed on the SEM stub were coated with a layer of Au/Pd to eliminate the charging problem. The average diameter of fibers was

defined following SEM imaging by using ImageJ software upon calculating ~100 fibers for each sample.

The inclusion complex formation within naproxen/HPβCD nanofibrous films were confirmed using different techniques. Firstly, attenuated total reflectance Fourier transform infrared spectroscopy (ATR-FTIR, PerkinElmer, USA) was used for this purpose. The FTIR spectra of nanofibrous films and pure naproxen were recorded with 32 scans in the range of 4000-600 cm⁻¹ and at a resolution of 4 cm⁻¹. X-ray diffraction (XRD, Bruker D8 Advance ECO, Germany) also established the IC formation within nanofibrous films by analyzing the conversion of naproxen crystals into the amorphous state by complexation. XRD measurements of nanofibrous films and naproxen were performed in the range of $2\theta = 5-30^{\circ}$ using Cu-K α radiation at 40 kV and 25 mA. The amorphization of naproxen was also confirmed using a differential scanning calorimeter (DSC, TA Instruments Q2000, USA). The DSC thermograms were obtained by heating samples which were placed in a T-zero Al pan from 0 °C to 200 °C using a 10 °C min⁻¹ heating rate. On the other hand, a thermal gravimetric analyzer (TGA, TA Instruments Q500, USA) provided the thermal degradation profile of samples which were located on the platinum pan and heated in the range of RT-500 °C in increments of 20 °C min⁻¹.

Loading efficiency

To calculate the loading efficiency of naproxen/HPβCD (1/1) IC and naproxen/HPβCD (1/2) IC nanofibrous films, ~1 mg of samples were dissolved in 5 mL of DMSO. Here, DMSO was selected to ensure the complete dissolution of components of naproxen and HPβCD within nanofibrous films. The naproxen content was measured using UV-vis spectroscopy (Perkin Elmer, Lambda 35, USA) (274 nm) and the calibration curve of naproxen in DMSO was obtained with $R^2 \ge 0.99$. The loading efficiency (%) was calculated by using the following formula;

Loading efficiency (%) =
$$Ce/Ct \times 100$$
 (Formula 1)

where Ce is the concentration of loaded naproxen and Ct is the initial concentration of naproxen in the nanofibrous films. The measurements were repeated three times to attain an average \pm standard deviation of results. Proton nuclear magnetic resonance spectroscopy (1H-NMR) was also operated to analyze the chemical structure and to determine the loading efficiency of nanofibrous films roughly. For this, naproxen/HPβCD (1/1) IC and naproxen/HPβCD (1/2) IC nanofibrous films and naproxen were separately dissolved in d_6 -DMSO, and then placed in a 1 H-NMR spectrometer (Bruker AV500, with an autosampler) for recording the ¹H-NMR spectra (16 scans). The results were examined by using Mestrenova software to calculate molar ratios through integrating characteristic peaks of components.

2D-NMR measurement

The rotating frame Overhauser effect spectroscopy (ROESY) method was applied to examine inclusion complex formation

between HPBCD and naproxen. Here, 2D-NMR measurement was performed using a 600 MHz Varian INOVA nuclear magnetic resonance spectrometer in D₂O at 25 °C.

Computational methodology

To reveal the inclusion complex formation mechanisms at the atomic scale, ab initio quantum mechanical calculations based on density functional theory⁴⁰ were performed using VASP software.41 The element potentials were described by the projector-augmented-wave method, and the size of the plane-wave basis set was determined by the kinetic energy cut-off, which was fixed to 520 eV. The exchange-correlation potential was approximated by the Perdew-Burke-Ernzerhof (PBE) form of generalized gradient approximation (GGA), and van der Waals interactions were taken into account by Grimme's dispersion correction (DFT-D2) method.⁴² The HPβCD, naproxen molecules, and their inclusion complexes were relaxed by the conjugate-gradient algorithm with precise energy (for self-consistent electronic steps) and force (for each ion) convergence criteria, which were 0.01 meV and 0.01 eV Å⁻¹, respectively. The solvent effect was included in calculations by the implicit solvation approach.⁴³

Pharmacotechnical properties

The phase solubility profile of naproxen in the existence of CD was investigated by mixing the excess amount of naproxen (~6 mg) with increasing concentrations of HPβCD in the range of 0-32 mM in 5 mL of unbuffered water consequently showing pH in the range of 5.6-4.1. The mixtures were shaken on an orbital shaker (450 rpm) for 24 h at RT. Afterwards, the aqueous systems were filtered using a disposable PTFE filter (0.45 µm) and UV-vis spectroscopy was used to record the absorbance intensity of aliquots at 230 nm. The calibration curve $(R^2 \ge 0.99)$ of naproxen in water/ ethanol (7/3, v/v) was applied to convert absorbance intensity into concentration (mM). For each system, the measurements were performed three times (average ± standard deviation). In addition, the binding constant (K_S) was calculated using the linear part of the phase solubility diagram by applying the following formula:

$$K_{\rm S} = {\rm slope}/S_0(1 - {\rm slope})$$
 (Formula 2)

where S_0 is the intrinsic solubility of naproxen (~ 0.4 mM).

The in vitro time-dependent release profiles of naproxen/ HPβCD (1/1) IC and naproxen/HPβCD (1/2) IC nanofibrous films were analyzed in PBS buffer having pH 7.4. For this, ~10 mg of samples were immersed in 10 mL of buffer solution and shaken on an orbital shaker at 200 rpm and 37 °C. Aliquots of 100 µL were taken from each sample system at particular time intervals (30 s to 10 min) and then 100 μL of fresh PBS buffer was readded into the same systems. For each sample, tests were repeated three times (average ± standard deviation) and the absorbance intensity of removed aliquots was measured using UV-vis spectroscopy (230 nm).

The calibration curve $(R^2 \ge 0.99)$ of naproxen in PBS/ethanol (7/3, v/v) was applied to convert absorbance intensity into release concentration (ppm). As the control, the release profile of pure naproxen (~1.3 mg) in the buffer system (pH 7.4, 10 mL) was also examined using a drug concentration of ~ 0.6 mM which is higher than its intrinsic solubility (~ 0.4 mM) and corresponds to the initial drug content of ~10 mg of naproxen/HPβCD (1/1) IC nanofibrous film. The release behaviour of the samples was also analyzed from the point of view of release kinetics by using different kinetic calculation models (see the ESI†).

The dissolution profiles of naproxen (~0.7 mg) and nanofibrous films (~5 mg) of HPβCD, the naproxen/HPβCD (1/1) IC and the naproxen/HPβCD (1/2) IC were examined by placing each sample in a vial and then adding 5 ml PBS to each of the vials. A simultaneous video was recorded to follow the dissolution behaviour (Video S1†). Here, the concentration of nanofibrous films (~1 mg mL-1) was kept the same with an in vitro release test. On the other hand, the evaluation of the disintegration profile was carried out in a medium that emulated the oral cavity moist environment. For this, filter paper (Fisherbrand, P5 Grade, Ø: 7 cm, medium porosity, cellulose) was placed on Petri dishes (Ø: 10 cm) and saturated with 10 mL of the artificial saliva solution. 10 Afterwards, an excess amount of medium was removed from the Petri dishes and then nanofibrous films of HPβCD, the naproxen/HPβCD (1/1) IC and the naproxen/ HPβCD (1/2) IC (\sim 6 × 7 cm) were placed individually on the wetted filter paper. Video S2† was concurrently recorded to reveal the disintegration behaviour of samples in the artificial saliva environment.

Statistical analyses

The statistical analyses were performed through Origin Lab (Origin, 2023, USA). The one-way or two-way of variance (ANOVA) was applied with a 0.05 level of probability.

Results and discussion

Morphology of nanofibrous films

Fig. 2 shows the photos of electrospinning solutions and ultimate HPβCD, naproxen/HPβCD (1/1) IC and naproxen/ HPβCD (1/2) IC nanofibrous films electrospun from these solutions along with their representative SEM images. Here, the HPBCD system was obtained as a clear solution (Fig. 2a-i) while the naproxen/HPβCD (1/1) IC system yielded a turbid one that was an indicator of the uncomplexed crystal naproxen existence in the solution (Fig. 2b-i). On the other hand, a clear solution was observed for the naproxen/HPβCD (1/2) IC system (Fig. 2c-i) just as in the HPβCD solution due to full complexation occurring between the drug and CD molecules in the aqueous solution. From all these three systems, free-standing, lightweight, and easily folded nanofibrous films were generated as a result of the electrospinning process as shown in Fig. 2a-c-i. The beadfree and uniform fiber formation for HPβCD, naproxen/

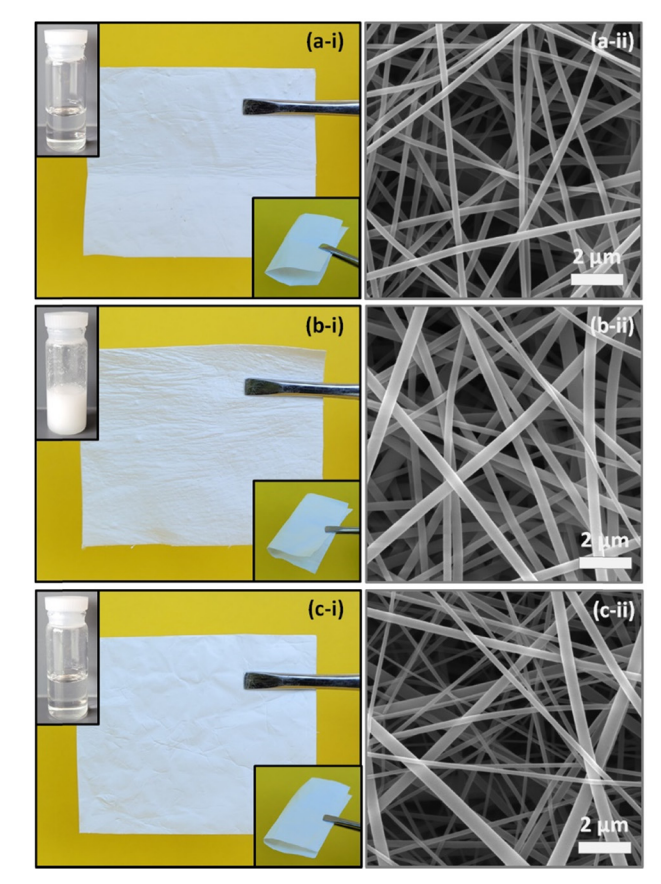


Fig. 2 (i) Photos of electrospinning solution and nanofibrous films and (ii) SEM images of nanofibrous films of (a) HPBCD, (b) the naproxen/ HP β CD (1/1) IC and (c) the naproxen/HP β CD (1/2) IC.

HPβCD (1/1) IC and naproxen/HPβCD (1/2) IC nanofibrous films was demonstrated using SEM imaging (Fig. 2a-c-ii).

The average fiber diameter (AFD) calculated from the SEM images and the solution properties including viscosity and conductivity are summarized in Table 1. As confirmed by the SEM images, thicker fibers were obtained for the naproxen/ HPβCD (1/1) IC nanofibrous film (260 \pm 70 nm) compared to the naproxen/HP β CD (1/2) IC (180 \pm 90 nm) and HP β CD (195 ± 45 nm) nanofibrous films (Table 1). The statistical analyses also depicted that the AFD of the naproxen/HPBCD (1/1) IC nanofibrous film was significantly different from the others (p < 0.05). The naproxen/HP β CD (1/1) IC system showed the highest viscosity (1.103 Pa s) and lowest conductivity (40.95 μS cm⁻¹) among the other two systems. This can be the explanation for thicker fiber formation than HPBCD and naproxen/HPβCD (1/2) IC nanofibrous films since a lower amount of electrical charge was formed in the naproxen/ HPβCD (1/1) IC solution and it led to less stretching during electrospinning (Table 1).44

Structural characterization

FTIR analysis can offer an understanding of interactions between guest and CD molecules by inclusion complexation

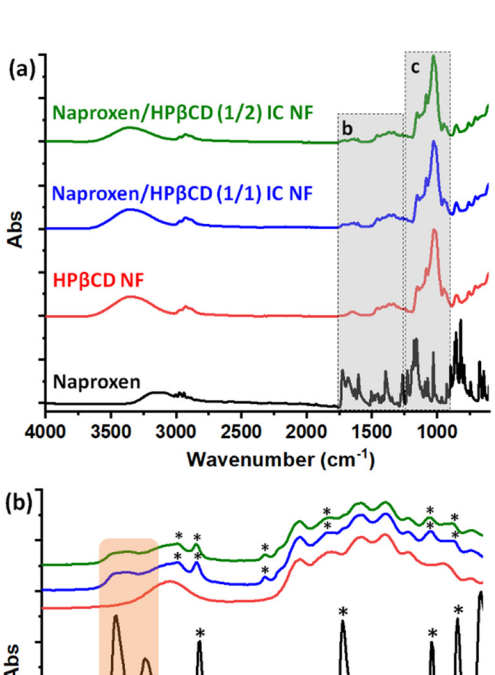
Table 1 Solution properties and average fiber diameters (AFD, average ± std deviation) of electrospun nanofibers

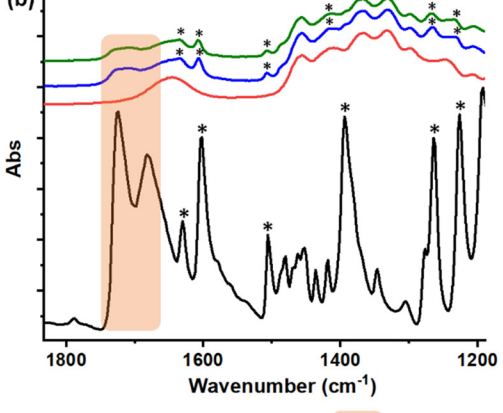
Sample	HPβCD conc. ^a (%, w/w)	Naproxen conc. ^b (%, w/w)	Viscosity (Pa s)	Conductivity (µS cm ⁻¹)	AFD (nm)
НРβCD	180	_	0.877	44.26	195 ± 45
Naproxen/HPβCD (1/1)	180	13.3	1.103	40.95	260 ± 70
Naproxen/HPβCD (1/2)	180	7.1	1.064	45.48	180 ± 90

^a With respect to the solvent. ^b With respect to the total sample amount.

which can result in shifts or disappearances of the characteristic peaks of components. 45 Here, Fig. 3 depicts the full and expanded FTIR graphs of naproxen and nanofibrous films of HPβCD, the naproxen/HPβCD (1/1) IC and the naproxen/HPβCD (1/2) IC. The FTIR spectra of the HPβCD nanofibrous film indicated characteristic bands belonging to HPβCD: 3350 cm⁻¹ (stretching vibration of O-H), 2930 cm⁻¹ (anti-symmetric vibration of CH₃), 1650 cm⁻¹ (bending vibration of O-H), 1150 cm⁻¹ (stretching vibration of C-O), and 1023 cm⁻¹ (stretching of the antisymmetric C-O-C glycosidic bridge) (Fig. 3a). 46 The distinct characteristic peaks of HPBCD were also detected in the FTIR spectra of the naproxen/HPβCD IC nanofibrous film due to the higher portion of CD content in the film structure ($\sim 87-93\%$ (w/w)). For pure naproxen, the characteristic absorption peaks were observed at 1724-1682 cm⁻¹ (-C=O stretching), 1602 cm⁻¹ and 1505 cm⁻¹ (C=C aromatic stretching), 1393 cm⁻¹ (CH₃ bending), 1264 and 1027 cm⁻¹ (symmetric aryl-O stretching), and 1225 cm⁻¹ (-O- stretching) (Fig. 3b and c). 30,31,39 All given characteristic peaks of naproxen were also observed in the FTIR graphs of naproxen/HPBCD (1/1) IC and naproxen/ HPβCD (1/2) IC nanofibrous films and this proved the existence of naproxen molecules in these samples (Fig. 3b and c). Moreover, there was a shift noticed for the characteristic peaks of naproxen in the case of the naproxen/ HPβCD IC nanofibrous films from 1631 cm⁻¹, 1602 cm⁻¹, 1505 cm⁻¹, 1393 cm⁻¹, 1264 cm⁻¹ and 1225 cm⁻¹ to 1634 ${\rm cm}^{-1},\,1607~{\rm cm}^{-1},\,1507~{\rm cm}^{-1},\,1417~{\rm cm}^{-1},\,1265~{\rm cm}^{-1}$ and 1230cm⁻¹, respectively (Fig. 3b). This confirmed the inclusion complex formation between naproxen and HPBCD in both electrospun nanofibrous films of the naproxen/HPβCD ICs.

In this study, XRD was utilized to examine the potential transition of naproxen crystals into the amorphous state as a result of the inclusion complex formation with HPBCD. Fig. 4a shows the XRD graphs of naproxen and nanofibrous films of HPβCD, the naproxen/HPβCD (1/1) IC and the naproxen/HPβCD (1/2) IC. The distinct characteristic peaks of naproxen at 6.5°, 12.6°, 16.8°, 19.0°, 20.4°, 22.5° and 23.7° exhibited the crystalline nature of this drug. 47 On the other hand, broad halos (10° and 18.5°) were detected in the case of the HPβCD nanofibrous film owing to its amorphous state. For the naproxen/HPβCD (1/1) IC nanofibrous film, the characteristic peaks of naproxen were observed demonstrating the existence of uncomplexed crystal drug parts within the sample. In contrast, the naproxen/HPBCD (1/2) IC nanofibrous film displayed an amorphous pattern identical to the pristine





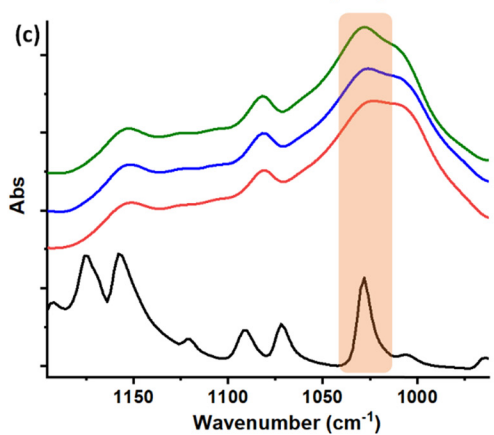


Fig. 3 (a) Full and (b and c) expanded FTIR graphs of naproxen, the HPβCD NF, the naproxen/HPβCD (1/1) IC NF and the naproxen/HPβCD (1/2) IC NF (nanofibrous film: NF).

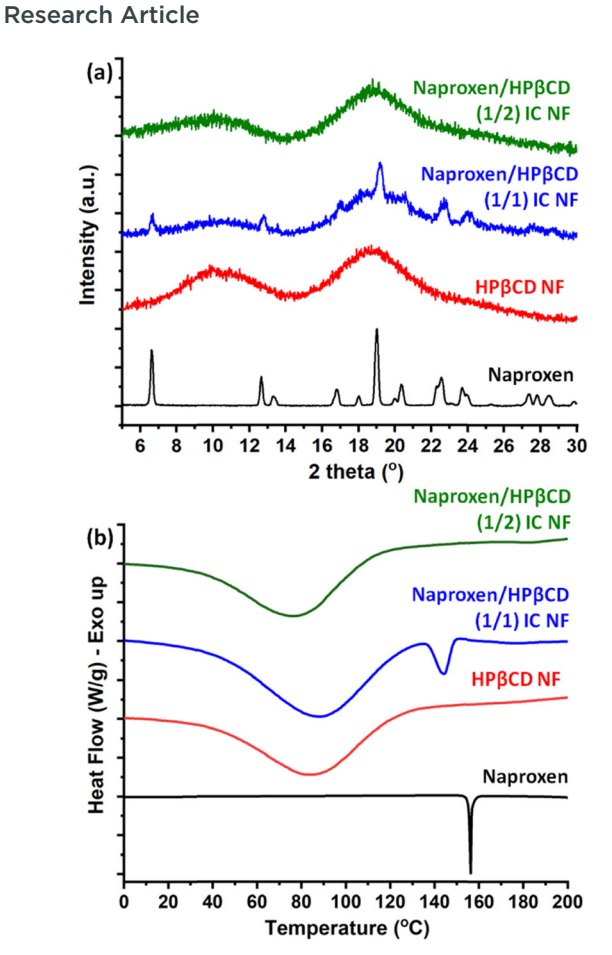


Fig. 4 (a) XRD and (b) DSC graphs of naproxen, the HPβCD NF, the naproxen/HPβCD (1/1) IC NF and the naproxen/HPβCD (1/2) IC NF (nanofibrous film: NF).

HPβCD nanofibrous film as a result of complete complexation between naproxen and HPBCD which ensured the full amorphization of drug crystals within the film.

The amorphous distribution of naproxen in the naproxen/ HPβCD (1/2) IC nanofibrous film and the presence of drug crystals in the naproxen/HPβCD (1/1) IC nanofibrous film were further verified using the DSC technique. Fig. 4b shows the DSC thermograms of naproxen and nanofibrous films of HPβCD, the naproxen/HPβCD (1/1) IC and the naproxen/ HPβCD (1/2) IC. Here, the DSC thermogram of naproxen showed an endothermic peak at ~156 °C corresponding to the melting of drug crystals.⁴⁷ On the other hand, both HPβCD and naproxen/HPβCD (1/2) IC nanofibrous films exhibited a broad endothermic peak at ~90 °C originating from dehydration of water content in the samples. The melting peak of naproxen was detected at around 144 °C with a broader feature compared to pure naproxen in the case of the naproxen/HPβCD (1/1) IC nanofibrous film, and this is evidence for the existence of both complexed and uncomplexed naproxen within the 1/1 based nanofibrous film. 45 Nonetheless, there was no distinct endothermic peak detected at the respective region of the thermogram for the naproxen/HPβCD (1/2) IC nanofibrous film supporting the

complete complexation between naproxen and HPBCD (Fig. 4b). It is obvious that the results of DSC aligned with both XRD findings (Fig. 4a) and visual observations of solution photos (Fig. 2).

Here, the TGA technique was applied to investigate the thermal degradation profile of the nanofibrous films. Fig. 5 shows the TGA thermograms and derivative thermograms (DTG) of naproxen and nanofibrous films of HPBCD, the naproxen/HPβCD (1/1) IC and the naproxen/HPβCD (1/2) IC. For the nanofibrous films, the weight-loss step completed at around 100 °C corresponded to the water dehydration from the samples. On the other hand, the main weight-loss observed at ~360 °C was due to the thermal degradation of HPβCD within the nanofibrous films (Fig. 5a). Differently from the pristine HPBCD nanofibrous film, an additional step was observed at ~305 °C in the case of the naproxen/ HPβCD IC ones which arose from the naproxen content (Fig. 5b). However, it is obvious that the thermal degradation of naproxen occurred at a higher temperature for the naproxen/HPβCD IC nanofibrous films when compared to pure naproxen degradation that happened at around 255 °C (Fig. 5b).³³ This shift also confirmed the inclusion complex formation between naproxen and HPBCD which required a higher level of energy for the thermal degradation process. TGA analysis can also provide information about the

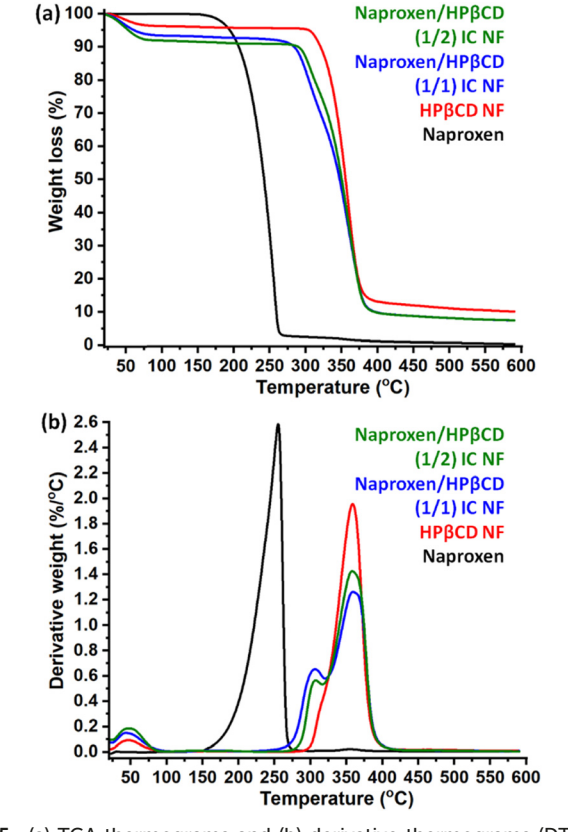


Fig. 5 (a) TGA thermograms and (b) derivative thermograms (DTG) of naproxen, the HPβCD NF, the naproxen/HPβCD (1/1) IC NF and the naproxen/HPβCD (1/2) IC NF (nanofibrous film: NF).

approximate content (%) of components within the samples. Here, the TGA thermograms of the naproxen/HPβCD IC nanofibrous films did not allow this calculation since the thermal degradation of naproxen overlapped with the main degradation of HPBCD. Even so, the DTG graphs clearly exhibited the differences in naproxen and HPBCD contents between the naproxen/HPβCD (1/1) IC and naproxen/HPβCD (1/2) IC nanofibrous films. Such that, the step intensity of naproxen was found to be lower in the case of the naproxen/ HPβCD (1/2) IC nanofibrous film compared to the naproxen/ HPβCD (1/1) IC one while it was higher for the HPβCD weight-loss step. This finding supported the lower drug content of the naproxen/HPBCD (1/2) IC nanofibrous film (~7.1%, w/w) than that of the naproxen/HPβCD (1/1) IC nanofibrous film (~13.3%, w/w).

Loading efficiency of nanofibrous films

The electrospinning solutions of naproxen/HPβCD IC systems were prepared using 1/1 and 1/2 molar ratios (drug/CD) that respectively corresponded to 13.3% and 7.1% (w/w) naproxen content in the electrospun nanofibrous films. The loading efficiency test revealed that the ultimate nanofibrous films of the naproxen/HPβCD (1/1) IC and naproxen/HPβCD (1/2) IC were respectively obtained with 83.73 \pm 4.36% and 100.03 \pm 3.51% (w/w) loading efficiency that corresponded to ~11.1% and ~7.1% (w/w) naproxen content. The statistical analyses also demonstrated the significant difference between the samples (p < 0.05). In other words, there was detected a slight loss of naproxen in the case of the naproxen/HPβCD (1/1) IC nanofibrous film and this most likely originated from the uncomplexed parts of drug molecules which caused heterogeneity in its electrospinning solution. On the other hand, no drug loss was noticed for the naproxen/HPβCD (1/2) IC nanofibrous film owing to the complete complexation attained between naproxen and HPBCD within the sample.

Here, ¹H-NMR analysis was also performed to examine the chemical structure and rough content of naproxen molecules within nanofibrous films. Fig. 6 shows the ¹H-NMR spectra of naproxen and nanofibrous films of the naproxen/HPβCD (1/1) IC and naproxen/HPβCD (1/2) IC. It was found that the characteristic peaks of naproxen presented the same pattern in the ¹H-NMR spectra of the naproxen/HPβCD (1/1) IC and naproxen/HPβCD (1/2) IC nanofibrous films. demonstrated the preserved chemical structure of this drug molecule during the whole process. On the other hand, the highlighted parts signified the non-overlapped integrated peaks of naproxen and HPBCD which were used to calculate the molar ratio of the ultimate nanofibrous films (Fig. 6). For naproxen, the peaks located between 7 ppm and 8 ppm corresponding to the aromatic ring of the molecule were taken into account during the calculation.³⁹ For HPβCD, the peak located at ~1 ppm corresponding to the methyl group was used for the analysis.20 The results revealed that the molar ratio (drug/CD) was found to be 1.00/1.04 and 1.00/ 1.97 for the naproxen/HPβCD (1/1) IC and naproxen/HPβCD

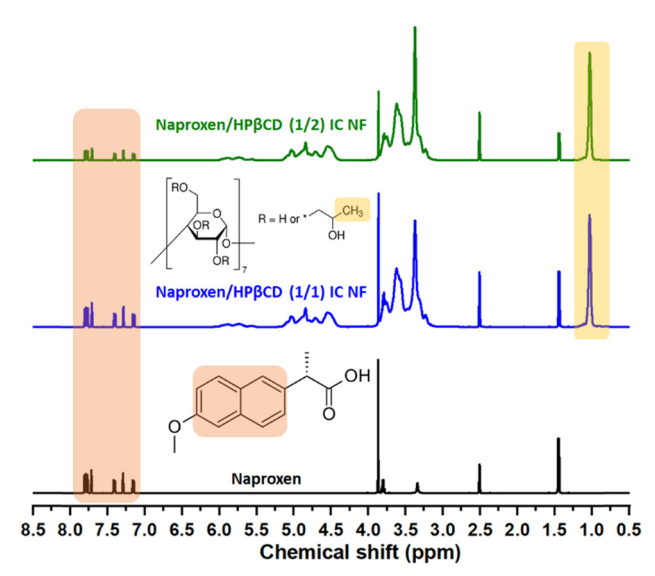


Fig. 6 ¹H-NMR spectra of naproxen, the naproxen/HPβCD (1/1) IC NF and the naproxen/HPβCD (1/2) IC NF (nanofibrous film: NF).

(1/2) IC nanofibrous films, respectively, corresponding to \sim 96.1% and \sim 101.5% (w/w) loading efficiency. These findings are approximately the same as the results of the loading efficiency test; however, the difference distinguished for the naproxen/HPβCD (1/1) IC nanofibrous film might be due to the variations between test techniques. Briefly, naproxen was effectively encapsulated into nanofibrous films with different loading contents (~7-11%, w/w) due to inclusion complexation between drug and CD molecules.

2D-NMR (ROESY) analysis

The ROESY technique enables probing interactions over extended distances up to 5 Å, so it is distinguished for the investigation of nanoscale assemblies constructed with CD.48 Therefore, 2D-NMR (ROESY) measurement was also performed to examine the spatial interactions within the inclusion complexes of naproxen and HPBCD. Fig. 7 depicts the existence of spatial interaction between the H atoms of host and guest molecules by the cross-peaks. The expanded ROESY spectra (Fig. 7b) were the evidence of concurrent proton resonances between the inner cavity protons (H₃ and H₅) of HPβCD and the aromatic protons of naproxen. In other words, the ROESY finding further revealed that the aromatic part of naproxen was encapsulated in the hydrophobic cavity of HPBCD by inclusion complexation.

Computational analysis

The interaction between naproxen and HPBCD and the formation of ICs were examined by first-principles computational methods. First, the ground state configurations of naproxen and HPBCD were obtained individually by relaxing structures in a vacuum. Next, the interaction between them was analyzed by varying the position and orientation of naproxen. The gradual decrease in total energy as naproxen approaches

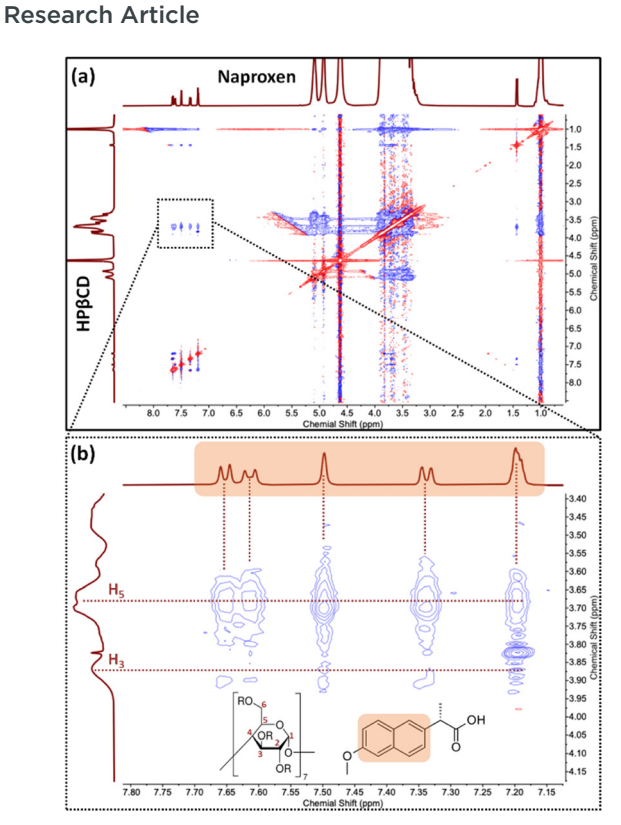


Fig. 7 (a) Full and (b) expanded 2D-NMR (ROESY) spectra of naproxen and HPβCD recorded in D₂O.

HPβCD indicated that interaction was energetically favourable and providing activation energy was not required for binding. While ICs can be formed for tail (T) and head (H) horizontal orientations of naproxen, vertical arrangements did not fit due to size match. The ground state configurations for 1:1 stoichiometry, where the total energy was minimum and the force acting on the system was practically zero (below 0.01 eV \mathring{A}^{-1} , which was set as a threshold value), are shown in Fig. 8a and b. At this point, complexation energy (E_{CE}) , which can be used to quantify the interaction strength, can be calculated as:

$$E_{\text{CE}} = n \times E_{\text{T}}[\text{HP}\beta\text{CD}] + E_{\text{T}}[\text{naproxen}]$$

- $E_{\text{T}}[\text{naproxen/HP}\beta\text{CD IC}]$ (Formula 3)

where $E_T[HP\beta CD]$, $E_T[naproxen]$, and $E_T[naproxen/HP\beta CD IC]$ are the total energies (calculated in a vacuum or solvent) of HP β CD, naproxen, and the naproxen/HP β CD IC, respectively. nindicates the number of HP β CD in the IC, which was 1 for 1:1 and 2 for 1:2 stoichiometry. The computed values are listed in Table 2. Positive values of E_{CE} point out the stability of the complex, and the T-orientation through the wide rim (B) was energetically the most favourable configuration for 1:1 stoichiometry. Similarly, 1:2 stoichiometry was also examined, and four stable designs are shown in Fig. 8c-f. The obtained $E_{\rm CE}$ values were significantly larger than 1:1, implying that 1:2 was the preferred stoichiometry for the naproxen/HPβCD IC. It should also be noted that the penetration through the narrow rim (A) reduces E_{CE} due to the HP arms. As a next step, the

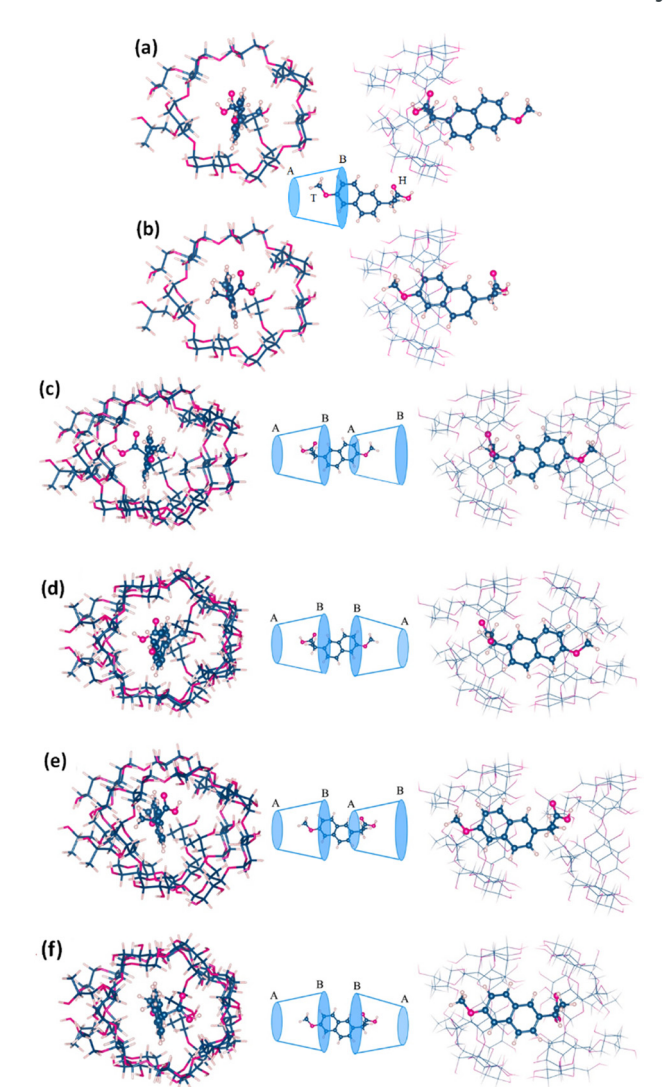


Fig. 8 The top and side views of the naproxen/HP β CD IC in (a) B-T and (b) B-H orientations for 1:1 stoichiometry and (c) B-HT-A, (d) B-HT-B, (e) B-TH-A and (f) B-TH-B orientations for 1:2 stoichiometry.

computations were repeated in water to reveal the influence of solvent on the attained properties. While the effect of water on structures was found to be minute, a notable decrease in $E_{\rm CE}$ was recognized (Table 2). This decrease marked a reduction in the binding strength between naproxen and HPβCD. Once the total energies of the structures and IC were calculated, the solvation energy (E_{SE}) of the system can be estimated. E_{SE} is defined as:

$$E_{\rm SE} = E_{\rm T}^{\rm Solv} - E_{\rm T}^{\rm Vac}$$
 (Formula 4)

where $E_{\mathrm{T}}^{\mathrm{Solv}}$ and $E_{\mathrm{T}}^{\mathrm{Vac}}$ are the total energy of the IC in water and a vacuum, respectively. As can be seen from Table 2, the $E_{\rm SE}$ of the naproxen molecule increased from -9.5 kcal mol⁻¹ up to -72.2 kcal mol⁻¹ and -104.0 kcal mol⁻¹ for 1:1 and 1:2 stoichiometries, respectively. The increase in $E_{\rm SE}$, in addition to a decrease in $E_{\rm CE}$ in water, signals an enhancement in solubility.

-103.69

E_{CE} (kcal mol⁻¹) E_{CE} (kcal mol⁻¹) Drug: CD Orient. $E_{\rm SE}$ (kcal mol⁻¹) 1:1 В-Н 6.25 -72.16B-T 8.18 5.01 1:2 B-HT-A 31.40 B-HT-B 28.64 -104.0465.80 B-TH-A 24.38

66.84

29.34

Table 2 The complexation and solvation energies of the naproxen/HPβCD IC for different orientations (orient.) in 1:1 and 1:2 stoichiometries (drug: CD). T and H indicate the tail and head orientations of naproxen; A and B indicate the narrow and wide rims of HPBCD (see Fig. 8)

Pharmacotechnical profiles of nanofibrous films

В-ТН-В

The effect of increasing HPβCD concentrations against naproxen solubility was examined by a phase solubility test (Fig. 9a). The intrinsic solubility of naproxen in the absence of the HPβCD molecule was ~0.4 mM and ~12.3 times higher solubility was attained for the highest HPβCD concentration of 32 mM by inclusion complexation. From the linear part of the phase solubility diagram, the binding constant (K_S) between naproxen and HPβCD was also calculated to be 588 M⁻¹. As is shown in Fig. S1,† the pH of the phase solubility test solutions decreased from 5.6 to 4.1 as the HPBCD concentration increased from 0 to 32 mM. Here, the decline observed at the pH values can be attributed to the increasing amount of solubilized naproxen in the aqueous systems by inclusion complexation since naproxen is a weak acid compound with a pK_a 4.2 value.⁴⁹ The other related reports in which the inclusion complexes of naproxen and HP β CD were studied revealed different K_S values. For instance, $K_{\rm S}$ values were reported to be 2080 ${\rm M}^{-1}$ and 2083 M⁻¹ for unbuffered systems in which pH was recorded at around 4.5³⁵ and 5,³⁷ respectively. On the other hand, 1123 M⁻¹ and 624 M⁻¹ were observed for buffer-based systems, respectively, having pH 730 and 1.50 In another related study of Cirri et al., K_S values were found to be 4890 M⁻¹, 2605 M⁻¹ and 230 M⁻¹ for buffered systems with 1.1, 4.0 and 6.5 pH values, respectively.⁴⁹ Here, the K_S of the naproxen/HPβCD couple decreased as the pH value increased and this was assigned to the progressive increase of the naproxen ionized form that shows a lower affinity for the apolar hydrophobic cavity of HPBCD. 49 However, it is still obvious that different K_S values can be obtained from the phase solubility analysis of the same host-guest (CD: drug) system. These variations can be ascribed to differences in the purity degree of molecules, CD concentration ranges used in the experiments, and/or the substitution degree of HPβCD. 49,51,52

In this study, the time dependent release of naproxen from the naproxen/HPβCD (1/1) IC and naproxen/HPβCD (1/2) IC nanofibrous films was examined in a PBS buffer system having pH 7.4. Fig. 9b shows the release graphs of nanofibrous films compared with pure naproxen. As is seen, the naproxen/HPβCD (1/2) IC nanofibrous film reached a release concentration of 65.72 ± 7.01 ppm in 30 seconds, showed an almost plateau profile over 10 minutes, and completed this period with 69.44 \pm

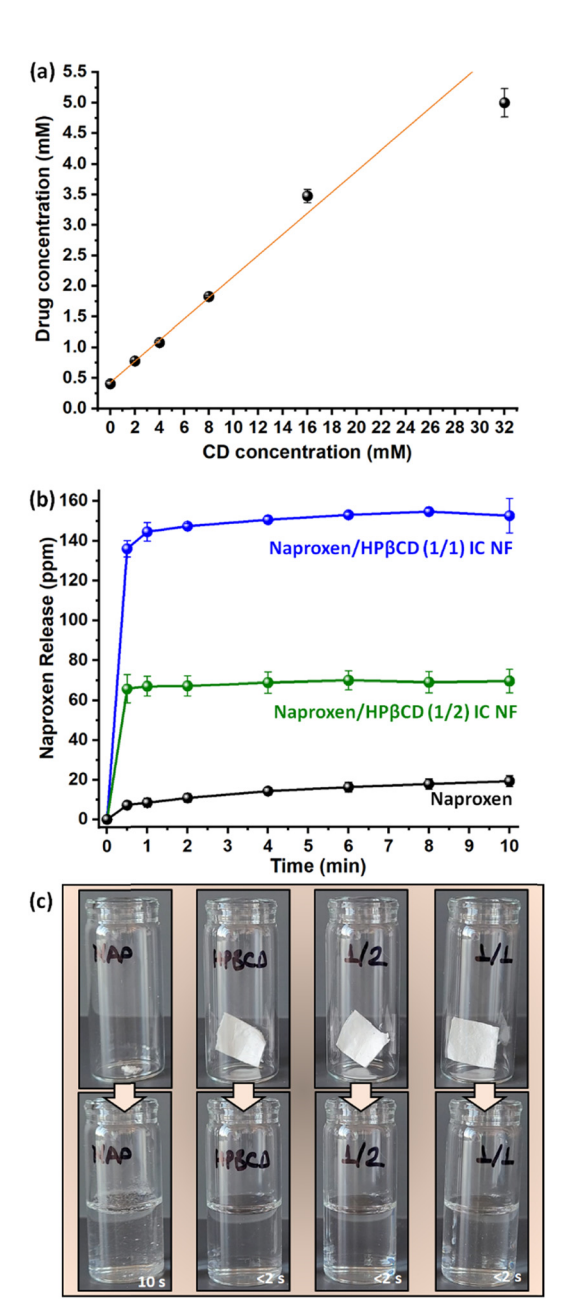


Fig. 9 (a) Phase solubility diagram of naproxen against increasing HPβCD concentrations. (b) In vitro time-dependent release profile of naproxen, the naproxen/HPβCD (1/1) IC NF and the naproxen/HPβCD (1/2) IC NF. (c) The dissolution profiles of (captured from Video S1†) naproxen, the HPβCD NF, the naproxen/HPβCD (1/1) IC NF and the naproxen/HPβCD (1/2) IC NF (nanofibrous film: NF).

Research Article

5.82 ppm of naproxen release (Fig. 9b). Here, the naproxen/ HPβCD (1/1) IC nanofibrous film also showed a fast release behaviour by releasing 136.05 \pm 4.12 ppm of naproxen in the first 30 seconds. Then, it reached a release concentration of 154.74 ± 1.65 ppm till the end of 10 minutes with a slightly increasing trend. On the other hand, pure naproxen displayed a release based on the dissolution of the drug in PBS buffer with a concentration of 7.24 ± 1.94 ppm in the first 30 seconds, and reached a release of 19.14 \pm 2.76 ppm at the end of 10 minutes (Fig. 9b). The remarkable difference between the samples was also established by the statistical analysis (p < 0.05). The variation between the released concentrations of the nanofibrous films was accordant with and proceeded from the naproxen content of the naproxen/HPβCD (1/1) IC (~13%, w/w) and naproxen/HPβCD (1/2) IC (~7%, w/w) systems. For the naproxen/HPβCD (1/1) IC nanofibrous film, the increment tendency detected on the release amount of naproxen in the given time period might be due to the time-dependent dissolution of drug crystals having an uncomplexed state existing in the samples. On the other hand, the inclusion complex formation between naproxen and HPBCD made it possible to reach enhanced and faster release of naproxen from the nanofibrous films compared to pure naproxen owing to the amorphous state and thus, improved water solubility of naproxen in the nanofibrous films. The notable aqueous solubility of HPβCD (>2000 mg mL⁻¹) can be also considered one of the main reasons to attain this better release profile in the case of nanofibrous films by their fast dissolution in the PBS medium. The dissolution profile of the samples was monitored visually as shown in Fig. 9c and Video S1.† Here, pure naproxen did not dissolve completely in PBS buffer due to its limited solubility, and undissolved particles remained floating in aqueous medium. In contrast, the nanofibrous films of HPβCD, the naproxen/HPβCD (1/1) IC and the naproxen/ HPβCD (1/2) IC instantly dissolved with the contact of the medium (Fig. 9c). While the naproxen/HPβCD (1/2) IC nanofibrous film dissolved close to that of the pure HPβCD nanofibrous film without remaining any particles, a few undissolved particles of naproxen were detected in the solution of the naproxen/HPβCD (1/1) IC nanofibrous film. This finding also reflected the whole amorphous state and incomplete inclusion complexation in the case of the naproxen/HPBCD (1/ 2) IC and naproxen/HPβCD (1/1) IC nanofibrous films, respectively.

The release behaviour of the samples was supplementarily inspected by various kinetic models. The formulations and their results (R^2 , regression coefficient) are given in the ESI† (Table S1). The kinetic model calculations demonstrated that the release profile of nanofibrous films did not adapt to the applied models of zero/first-order, Higuchi and Hixson-Crowell models (Table S1†). This showed that the release of naproxen was not coherent with Fick's first law displaying the time-dependent release from an insoluble matrix.⁵³ However, comparatively better consistency was detected with the Korsmeyer-Peppas model revealing the erosion and diffusion-controlled release of naproxen from the naproxen/HPβCD IC nanofibrous films. The release of naproxen

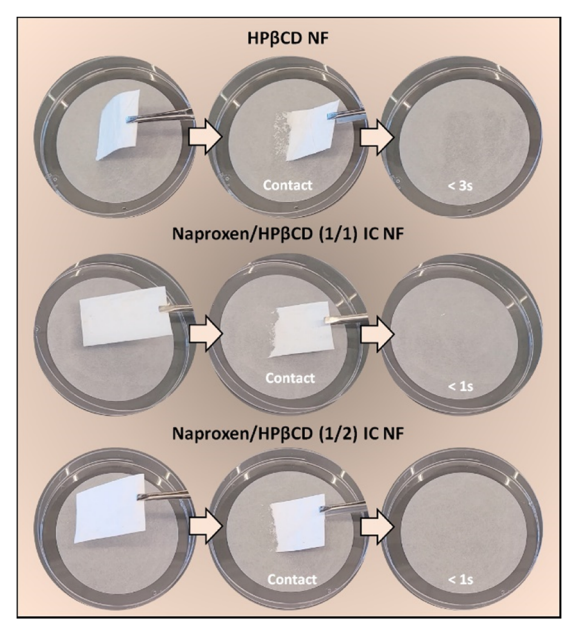


Fig. 10 Disintegration profiles of the HPβCD NF, the naproxen/HPβCD (1/1) IC NF and the naproxen/HPBCD (1/2) IC NF (captured from Video S2†) (nanofibrous film: NF).

presented consistency with almost all applied kinetic models by proving the prepotency of the Fickian diffusion mechanism and the progressive disintegration as a function of time for the release behaviour of this drug molecule. 53,54 The Korsmeyer-Peppas equation also enabled the calculation of the diffusion exponent (n) value, and it was detected in the range of 0.45 < n < 0.89 for all samples pointing out the irregular diffusion of naproxen into the aqueous medium.⁵³

For the examination of the disintegration profile, the moist environment of the oral cavity was simulated using filter paper which was saturated with an artificial saliva medium. 10 Fig. 10 shows the photos caught from Video S2.† It is obvious that the naproxen/HPβCD IC nanofibrous films were immediately absorbed by wetted filter paper in less than a second just after contact (Fig. 10). The impressive disintegration behaviour of nanofibrous films is essentially owing to unique properties including the highly water-soluble nature of HPBCD, and the high surface area and the high porosity of nanofibrous films which create additional access channels and active sides during the penetration of aqueous medium within fiber structures. Consequently, naproxen/HPBCD IC nanofibrous films would be appropriate fast-disintegrating delivery systems for oral applications by ensuring rapid release and disintegration features and without giving an unfavourable granular sense during treatments. This approach can be carried one step further by conceiving nanofibrous films having multi-phase release with an initial fast release profile. 55,56

Conclusions

In this study, polymer-free nanofibrous films of naproxen/ HPβCD ICs were generated with two different molar ratios of

1/1 and 1/2 (drug/CD) having a uniform morphology with ~260 nm and ~180 nm average fiber diameter, respectively. Naproxen/HPβCD IC nanofibrous films were obtained in water and in the absence of toxic chemicals. While full amorphous distribution of naproxen was provided in the naproxen/HPβCD (1/2) IC nanofibrous film due to complete complexation, uncomplexed naproxen parts were detected in the case of the naproxen/HPBCD (1/1) IC nanofibrous film. Accordingly, the naproxen/HPβCD (1/1) IC and naproxen/ HPβCD (1/2) IC nanofibrous films were respectively attained with ~84% and ~100% loading efficiency that corresponds to $\sim 11\%$ and $\sim 7\%$ (w/w) drug content. The complexation energy calculated by the modeling study also demonstrated a more favourable interaction between HPBCD and naproxen for the 1/2 molar ratio compared to 1/1 (drug/CD). Additionally, 2D-NMR (ROESY) results supported the complex formation between naproxen and HPβCD molecules by the encapsulation of the aromatic part of naproxen into the hydrophobic cavity of HPβCD. Here, the highly porous structure, high surface area and extremely high-water solubility of HPβCD (>2000 mg mL⁻¹) made possible the fast dissolution of naproxen/HPBCD IC nanofibrous films in water. The amorphous state of naproxen arising from inclusion complexation within nanofibrous films ensured a faster release for naproxen than its pure crystal form. In naproxen/HPβCD nanofibrous addition, IC disintegrated in the artificial saliva environment in less than a second. Briefly, the findings displayed that naproxen/ HPβCD IC nanofibrous films can be a promising alternative dosage form for the treatment of naproxen as an orally fastdisintegrating drug delivery system. Further research on electrospun nanofibrous films of different drugs using CD inclusion complexes would be valuable for the progress and understanding of these fast-disintegrating systems.

Author contributions

A. C. took part in the conceptualization, methodology, investigation and writing - original draft. K. D. took part in the investigation and writing - original draft. M. A. took part in the 2D-NMR and pH value investigation. M. E. K. and E. D. took part in the investigation - computational modeling and writing - computational modeling. T. U. took part in the conceptualization, methodology, editing, funding acquisition and project administration.

Conflicts of interest

There are no conflicts to declare.

Acknowledgements

This work made use of the Cornell Center for Materials Research Shared Facilities which are supported through the NSF MRSEC program (DMR-1719875), the Cornell Chemistry NMR Facility supported in part by the NSF MRI program (CHE-1531632), and the Department of Human Centered Design facilities. M. E. K. acknowledges support from the Brain Pool Program through the National Research Foundation of Korea (NRF) funded by the Ministry of Science and ICT (2020H1D3A1A02081517).

References

- 1 S. Kalepu and V. Nekkanti, Acta Pharm. Sin. B, 2015, 5, 442-453.
- 2 F. Ditzinger, D. J. Price, A.-R. Ilie, N. J. Köhl, S. Jankovic, G. Tsakiridou, S. Aleandri, L. Kalantzi, R. Holm and A. Nair, J. Pharm. Pharmacol., 2019, 71, 464-482.
- 3 M. He, L. Zhu, N. Yang, H. Li and Q. Yang, Int. J. Pharm., 2021, 604, 120759.
- 4 E. Turković, I. Vasiljević, M. Drašković and J. Parojčić, J. Drug Delivery Sci. Technol., 2022, 103708.
- 5 J. Boateng, J. Pharm. Sci., 2017, 106, 3188-3198.
- 6 M. Almukainzi, G. L. B. Araujo and R. Löbenberg, J. Pharm. Invest., 2019, 49, 229-243.
- 7 D.-G. Yu, J.-J. Li, G. R. Williams and M. Zhao, J. Controlled Release, 2018, 292, 91-110.
- 8 Y. Si, S. Shi and J. Hu, Nano Today, 2023, 48, 101723.
- 9 S. M. Tan, X. Y. Teoh, J. Le Hwang, Z. P. Khong, R. Sejare, A. Q. A. Al Mashhadani, R. Abou Assi and S. Y. Chan, J. Drug Delivery Sci. Technol., 2022, 103761.
- 10 B. Balusamy, A. Celebioglu, A. Senthamizhan and T. Uyar, J. Controlled Release, 2020, 326, 482-509.
- 11 H. Liu, Y. Dai, J. Li, P. Liu, W. Zhou, D.-G. Yu and R. Ge, Front. Bioeng. Biotechnol., 2023, 11, 1172133.
- 12 M. Wang, R.-L. Ge, F. Zhang, D.-G. Yu, Z.-P. Liu, X. Li, H. Shen and G. R. Williams, Biomater. Adv., 2023, 150, 213404.
- 13 H. Lv, Y. Liu, P. Zhao, Y. Bai, W. Cui, S. Shen, Y. Liu, Z. Wang and D.-G. Yu, Appl. Catal., B, 2023, 330, 122623.
- 14 S. Nam, S. Y. Lee and H.-J. Cho, J. Colloid Interface Sci., 2017, 508, 112-120.
- 15 N. Sharifi, S. A. Mortazavi, S. Rabbani, M. Torshabi, R. Talimi and A. Haeri, J. Drug Delivery Sci. Technol., 2022, 103356.
- 16 H. Bukhary, G. R. Williams and M. Orlu, Int. J. Pharm., 2018, 549, 446-455.
- 17 E. Hsiung, A. Celebioglu, R. Chowdhury, M. E. Kilic, E. Durgun, C. Altier and T. Uyar, J. Colloid Interface Sci., 2022, 610, 321-333.
- 18 E. Hsiung, A. Celebioglu, M. E. Kilic, E. Durgun and T. Uyar, Mol. Pharmaceutics, 2023, 20, 2624-2633.
- 19 M. Irfan, S. Rabel, Q. Bukhtar, M. I. Qadir, F. Jabeen and A. Khan, Saudi Pharm. J., 2016, 24, 537-546.
- 20 E. Hsiung, A. Celebioglu, M. E. Kilic, E. Durgun and T. Uyar, Int. J. Pharm., 2022, 623, 121921.
- 21 A. Celebioglu, N. Wang, M. E. Kilic, E. Durgun and T. Uyar, Mol. Pharmaceutics, 2021, 18, 4486-4500.
- 22 A. Celebioglu and T. Uyar, Mater. Sci. Eng., C, 2021, 118, 111514.
- 23 S. Gao, W. Feng, H. Sun, L. Zong, X. Li, L. Zhao, F. Ye and Y. Fu, J. Agric. Food Chem., 2022, 70, 7911-7920.
- 24 S. Gao, J. Jiang, X. Li, F. Ye, Y. Fu and L. Zhao, J. Agric. Food Chem., 2021, 69, 5871-5881.

- 25 S. Gao, X. Li, G. Yang, W. Feng, L. Zong, L. Zhao, F. Ye and Y. Fu, *Ind. Crops Prod.*, 2022, **176**, 114300.
- 26 S. Patil, A. Celebioglu and T. Uyar, J. Drug Delivery Sci. Technol., 2023, 85, 104584.
- 27 A. Celebioglu and T. Uyar, RSC Med. Chem., 2020, 11, 245–258.
- 28 P. Jansook, N. Ogawa and T. Loftsson, *Int. J. Pharm.*, 2018, 535, 272–284.
- 29 S. S. Braga, J. Drug Delivery Sci. Technol., 2022, 103650.
- 30 S. Mohandoss, N. Ahmad, M. R. Khan and Y. R. Lee, *J. Mol. Liq.*, 2023, 122411.
- 31 A. Mani, P. Ramasamy, A. A. M. Prabhu and N. Rajendiran, *J. Mol. Struct.*, 2023, **1284**, 135301.
- 32 S. Pereva, T. Sarafska, V. Petrov, S. Angelova and T. Spassov, J. Mol. Struct., 2021, 1235, 130218.
- 33 P. Mura, G. P. Bettinetti, M. Cirri, F. Maestrelli, M. Sorrenti and L. Catenacci, *Eur. J. Pharm. Biopharm.*, 2005, **59**, 99–106.
- 34 A. C. Illapakurthy, C. M. Wyandt and S. P. Stodghill, *Eur. J. Pharm. Biopharm.*, 2005, **59**, 325–332.
- 35 P. Mura, F. Maestrelli and M. Cirri, Int. J. Pharm., 2003, 260, 293–302.
- 36 B.-J. Lee and J.-R. Lee, Arch. Pharmacal Res., 1995, 18, 22-26.
- 37 F. Melani, G. P. Bettinetti, P. Mura and A. Manderioli, J. Inclusion Phenom. Mol. Recognit. Chem., 1995, 22, 131–143.
- 38 M. Séon-Lutz, A.-C. Couffin, S. Vignoud, G. Schlatter and A. Hébraud, *Carbohydr. Polym.*, 2019, **207**, 276–287.
- 39 M. F. Canbolat, A. Celebioglu and T. Uyar, *Colloids Surf.*, B, 2014, 115, 15–21.
- 40 G. Kresse and J. Furthmüller, *Comput. Mater. Sci.*, 1996, 6, 15–50.

- 41 G. Kresse and J. Furthmüller, *Phys. Rev. B: Condens. Matter Mater. Phys.*, 1996, 54, 11169.
- 42 S. Grimme, J. Comput. Chem., 2006, 27, 1787-1799.
- 43 K. Mathew, R. Sundararaman, K. Letchworth-Weaver, T. A. Arias and R. G. Hennig, *J. Chem. Phys.*, 2014, **140**, 84106.
- 44 J. Xue, T. Wu, Y. Dai and Y. Xia, *Chem. Rev.*, 2019, **119**, 5298–5415.
- 45 G. Narayanan, R. Boy, B. S. Gupta and A. E. Tonelli, *Polym. Test.*, 2017, 62, 402–439.
- 46 C. Yuan, B. Liu and H. Liu, *Carbohydr. Polym.*, 2015, **118**, 36–40.
- 47 B. Rojek, M. Gazda and A. Plenis, *Spectrochim. Acta, Part A*, 2023, 123048.
- 48 M. Haouas, C. Falaise, N. Leclerc, S. Floquet and E. Cadot, Dalton Trans., 2023, 52, 13467–13481.
- 49 M. Cirri, F. Maestrelli, G. Corti, S. Furlanetto and P. Mura, J. Pharm. Biomed. Anal., 2006, 42, 126–131.
- 50 J. Blanco, J. L. Vila-jato, F. Otero and S. Anguiano, *Drug Dev. Ind. Pharm.*, 1991, 17, 943–957.
- 51 S. Anguiano-Igea, F. J. Otero-Espinar, J. L. Vila-Jato and J. Blanco-Méndez, *Eur. J. Pharm. Sci.*, 1997, 5, 215–221.
- 52 T. Loftsson, H. Frikdriksdóttir, A. M. Sigurkdardóttir and H. Ueda, *Int. J. Pharm.*, 1994, **110**, 169–177.
- 53 N. A. Peppas and B. Narasimhan, J. Controlled Release, 2014, 190, 75-81.
- 54 R. Gouda, H. Baishya and Z. Qing, J. Dev. Drugs, 2017, 6, 1-8.
- 55 D.-G. Yu and J. Zhou, J. Pharm. Sci., 2023, 112, 2719–2723.
- 56 J. Zhou, P. Wang, D.-G. Yu and Y. Zhu, *Expert Opin. Drug Delivery*, 2023, **20**, 621–640.